JOURNAL OF CATALYSIS 89, 314–326 (1984)

# Adsorptive Properties of Magnetite Surfaces as Studied by Temperature-Programmed Desorption: Studies of $O_2$, NO, $CO_2$, and CO Adsorption

TERRENCE J. UDOVIC[1] AND J. A. DUMESIC[2]

*Department of Chemical Engineering, University of Wisconsin, Madison, Wisconsin 53706*

Received November 18, 1983; revised April 24, 1984

The adsorptive properties of magnetite surfaces of differing oxidation state were studied with respect to various probe molecules ($O_2$, NO, $CO_2$, and CO) using temperature-programmed desorption (TPD). Oxygen existed on these surfaces as molecular species ($Q_{O_2} \cong 61$ and 78 kJ mol$^{-1}$, where $Q$ is the heat of adsorption), atomic species, and lattice-like species. The number of these various oxygen species decreased as the surface was vacuum-annealed at higher temperatures. Correspondingly, the number and coordinative unsaturation of surface cations increased. Nitric oxide adsorbed as both weakly bound nitrosyl and strongly bound dissociated species. Nitrosyl species ($Q_{NO} \cong 60$–130 kJ mol$^{-1}$) desorbed as NO and simultaneously reacted to form a small amount (ca. 1%) of desorbed $N_2O$ and surface oxygen. Dissociated species reacted to form $N_2$ (with an activation energy of ca. 200 kJ mol$^{-1}$) and surface lattice oxygen. The surface coverages of both species increased with increasing extent of surface reduction, and total NO coverages correlated with the number of exposed cation sites. Carbon dioxide adsorbed as both monodentate ($Q_{CO_2} \cong$ 50–60 kJ mol$^{-1}$) and bidentate ($Q_{CO_2} \cong 60$–120 kJ mol$^{-1}$) carbonate species. Bidentate carbonate formation, which required cation–anion pair sites, inhibited NO adsorption on cation sites and was blocked by NO preadsorption on these sites. The $CO_2$ forming these carbonate species was capable of exchanging one oxygen with the surface upon desorption. Total $CO_2$ coverages correlated with the number of reactive surface oxygen species. Carbon monoxide weakly adsorbed ($Q_{CO} \cong 46$ kJ mol$^{-1}$) in a carbonyl fashion on cation sites of low coordination.

## INTRODUCTION

A variety of sites may exist on a metal oxide surface. These include coordinatively unsaturated cations, surface anions, and cation–anion pairs. A number of different adsorption modes may therefore exist for an adsorbate on a given metal oxide surface. In order to understand the adsorptive and catalytic properties of such a material, it is necessary to know which of these adsorption states are predominant on the surface. The present paper involves the use of temperature-programmed desorption (TPD) to probe the surface sites and adsorption states of $O_2$, NO, $CO_2$, and CO on magnetite ($Fe_3O_4$).

A previous paper (*1*) described the preparation and characterization of the magnetite surfaces which were used in the present study. These surfaces were formed by the oxidation of a polycrystalline metallic iron foil. The 30-nm iron oxide overlayer thereby formed was identified as magnetite through the use of conversion electron Mössbauer spectroscopy, and X-ray photoelectron spectroscopy was used to monitor the oxidation state of the magnetite surface. Of importance for the present study was the observation that the surface atomic ratios of $Fe^{2+}/Fe^{3+}$ and Fe/O could be controlled by vacuum-annealing the magnetite overlayer at temperatures from 300 to 675 K. This provided an experimental strategy for the present study of the adsorptive proper-

[1] Present address: U.S. Department of Commerce, National Bureau of Standards, Surface Science Division, Washington, D.C. 20234.

[2] To whom correspondence should be addressed.



0021-9517/84 $3.00

ties of magnetite as a function of the oxidation state of the surface.

## EXPERIMENTAL

Overlayers of magnetite on a polycrystalline iron foil (MRC, MARZ grade 99.99% purity) were formed by the oxidation treatment described in a previous paper (*1*) (i.e., $3 \times 10^{-4}$ Pa $O_2$, 673 K, 45 min). The oxidation state of the surface was controlled by a series of pretreatment steps, the final step of which involved vacuum-annealing at a temperature $T$. The determining feature of this procedure was shown elsewhere (*1*) to be the temperature $T$, at which the sample was vacuum-annealed following oxidation. Accordingly, the various magnetite surfaces used in the present study are designated by this evacuation temperature.

Temperature-programmed desorption (TPD) experiments on magnetite surfaces were performed in a bakeable stainless-steel UHV chamber (Perkin–Elmer Ultek, TNB-X system) pumped by a 200-liters $s^{-1}$ ion pump, a titanium sublimation pump, and a liquid-nitrogen cryopanel. Base pressures were typically $1 \times 10^{-8}$ Pa. This apparatus has been described in detail elsewhere (*2*). The sample was mounted on a rotary feedthrough. A Cu conductor feedthrough (12 kV, 150 A), a dual-tube liquid-nitrogen feedthrough, and a multiple thermocouple feedthrough were mounted next to this rotary feedthrough to aid in heating, cooling, and measuring the temperature of the sample. The sample mounting and heating design were adapted from similar systems reported in the literature (e.g., (*3*)). The sample (20 mm diameter and <0.125 mm thick) was suspended from a (spot-welded) 1-mm-diameter Fe support wire. A coiled tungsten filament situated ca. 3 mm behind the sample was used as a radiative heater during thermal treatments and desorption experiments, permitting heating rates greater than 70 K $s^{-1}$. Sample cooling to ca. 120 K was achievable by heat conduction through the Fe support wire to the stainless-steel holder cooled by liquid nitrogen. Through this arrangement, sample cooling from 1000 to 150 K could be achieved in 4 min. Sample temperature was monitored continuously with a (12 $\mu$m diameter) Chromel–Alumel thermocouple spot-welded to the back surface.

Temperature-programmed desorption spectra were collected in both line-of-sight (LS) and nonline-of-sight (NLS) modes, with respect to the mass spectrometer (UTI 100C), for identical surface and dosing pretreatments. Difference spectra (LS–NLS) were calculated to cancel spectral contributions equivalent in both modes of operation. These include nonline-of-sight desorption contributions from the back of the sample, the W filament, and the support surfaces as well as isotropic partial pressure contributions from the front of the sample. Assuming that the only significant difference between the two modes was the flux contribution due to line-of-sight desorption into the mass spectrometer ionizer, the difference spectra were treated as flux spectra.

Cracking patterns for the various gas species under consideration were experimentally determined and used to deconvolute desorption spectra possessing signal overlap from more than one mass fragment. Relative coverages of the different surface species were determined using appropriate relative mass spectrometer sensitivity factors. These factors were determined by an empirical calculation method suggested by UTI (*4*). Temperature-programmed desorption spectra were collected and stored in a UTI Programmable Peak Selector (PPS) for subsequent computer analysis.

Gas adsorption on the sample surface was accomplished by dosing through a 0.35-mm-i.d. stainless-steel syringe (located 25 mm from the sample surface), which reduced adsorption on the back surface of the sample as well as on the filament and support surfaces. Dosing was performed at constant backpressures behind the syringe. Effective dosing pressures

were determined by comparing desorption spectra with those from known isotropic exposures of the same gas. Pressures and exposures of each gas were calculated using appropriate ionization gauge sensitivity factors.

Argon (99.9995%), $CO_2$ (99.8%), and CO (99.5%) were obtained from Matheson. Oxygen (99.9%) was obtained from Chemetron. Nitrogen-15-labeled NO (99% $^{15}N$) was obtained from Prochem. Oxygen-18-labeled $O_2$ (99.51% $^{18}O$) and $C^{18}O_2$ (99.85% $^{18}O$) were obtained from Alfa Products. All gases were used without further purification.

## RESULTS AND DISCUSSION

### *TPD Calibration Experiments*

Before performing desorption experiments on the various model magnetite surfaces, the CO and $H_2$ adsorption behavior of the clean polycrystalline Fe surface was examined. This allowed comparison of the results of the present TPD experiments with the literature results (e.g., (*3, 5–8*)) to verify proper functioning of the TPD apparatus. Second, it permitted utilization of CO desorption flux spectra from Fe as calibration spectra for subsequently estimating all other coverages of adsorbed species on magnetite surfaces as well as for determining the ionization gauge sensitivity factor for CO.

The degreased Fe foil sample was mounted in the TPD chamber and cleaned by a procedure similar to the one described elsewhere (*1*). In short, after sputtering away the superficial oxide overlayer from the front face, the sample was vacuum-annealed at 1000 K for 30 min to reduce the amount of dissolved $N_2$, followed by numerous sputter-anneal cycles (sputter, 3 kV, 20 min; anneal, 825 K, 30 min). The TPD spectra subsequently collected for CO and $H_2$ were in excellent agreement with the reported behavior of these molecules on clean iron surfaces. Indeed, the resemblance of these TPD spectral results for the polycrystalline sample of this study to the published TPD spectral results for Fe(110) suggests that this sample was primarily composed of (110) surface planes. The reader is referred elsewhere for further details (*2*).

### *Interaction of $O_2$ with Magnetite Surfaces*

After the above calibration experiments, the sample was subjected to several sputter–anneal cleaning cycles to ensure cleanliness prior to formation of the magnetite overlayer via oxidation treatment. As mentioned previously, this was followed by further treatment of the sample to control the oxidation state of the surface. Desorption spectra of $O_2$ were then collected for these various magnetite surfaces immediately following preparation and cooling to 150 K. These spectra are illustrated in Fig. 1. Spectra from surfaces vacuum-annealed at temperatures higher than 250 K showed no $O_2$ desorption. The 250 K surface displays a single $O_2$ desorption peak at ca. 330 K (designated as the $\alpha_2$ state). The 150 K surface displays an additional $O_2$ desorption peak at ca. 260 K (designated as the $\alpha_1$ state). Assuming that the magnetite surface area was identical to the original metallic Fe surface area (i.e., no changes in microscopic surface roughness occurred upon oxidation), the total coverage of desorbable $O_2$ from

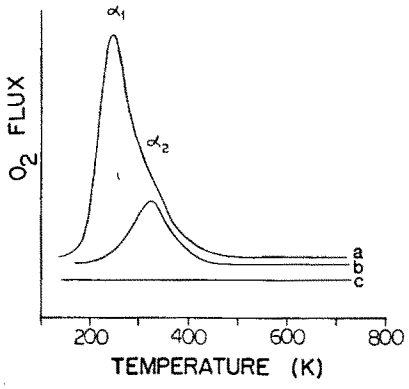


FIG. 1. TPD spectra (50 K $s^{-1}$) of $O_2$ desorption from various magnetite surfaces after cooling to 150 K: Samples vacuum-annealed at (a) 150 K, (b) 250 K, and (c) 300–900 K.

the 150 K surface was determined to be ca. $4.0 \times 10^{16}$ molecules $m^{-2}$ (ca. $2.7 \times 10^{16}$ and $1.3 \times 10^{16}$ molecules $m^{-2}$ in the $\alpha_1$ and $\alpha_2$ states, respectively). Desorption spectra of surfaces with different initial coverages of the $\alpha_1$ and $\alpha_2$ oxygen states indicated that the desorption peak positions remained invariant with changes in coverage, implying first-order desorption processes. Assuming preexponential factors of $10^{13}$ $s^{-1}$, desorption activation energies $E_d$ of 61 and 78 kJ $mol^{-1}$ were calculated for the $\alpha_1$ and $\alpha_2$ states, respectively. For nonactivated adsorption, these values are also equal to heats of adsorption, $Q_{O_2}$.

Other $O_2$ adsorption studies on iron oxides have indicated three states of adsorbed oxygen above ca. 250 K (*9–13*), the most-weakly-bound state being molecular and the other more-strongly-bound states being atomic. The desorption activation energy for the $\alpha_2$ state observed in the present study agrees well with that of the molecularly adsorbed $O_2^-$ species ($E_d$ = 77 kJ $mol^{-1}$) proposed on $\alpha$-$Fe_2O_3$ (*9*) and the $O_2^-$ species ($E_d$ = 81 kJ $mol^{-1}$) observed on $Fe_3O_4$ (*10*). There is no similar correspondence with the $\alpha_1$ state since high surface temperatures used in the other studies precluded its formation. This more-weakly-bound $\alpha_1$ state may be either an $O_2^-$ species or a more neutral $O_2$ species (*14*). The matching of the $\alpha_1$ and $\alpha_2$ states with adsorbed molecular species was further justified with the aid of $^{18}O_2$. A 150 K surface was prepared utilizing an equimolar mixture of $^{16}O_2$ and $^{18}O_2$. Similar desorption spectra for $^{16}O_2$ and $^{18}O_2$, combined with the absence of $^{18}O^{16}O$, indicated that no scrambling had occurred between $^{16}O_2$ and $^{18}O_2$ coadsorbing on the surface in the $\alpha_1$ and $\alpha_2$ states.

Assuming that the polycrystalline oxide surface is mainly composed of $Fe_3O_4$(100) crystal planes, the surface lattice oxygen density can be estimated to be $1.1 \times 10^{19}$ sites $m^{-2}$. Hence, the desorbable oxygen from the 150 K surface, $8.0 \times 10^{16}$ atoms $m^{-2}$, amounted to ca. 0.0073 lattice oxygen monolayers, a relatively small fraction. This quantity of desorbable $O_2$, however, does not necessarily coincide with the initial surface coverage of adsorbed species. In fact, reported $O_2$ adsorption studies on bulk iron oxide ($Fe_3O_4$ and $\alpha$-$Fe_2O_3$) specimens suggested that atomic oxygen species (such as $O^-$ and $O^{2-}$) were also present on the surface, desorbing above ca. 400 K (*9–13*). Thus, it appears that there is a competition for the fate of adsorbed oxygen species on magnetite surfaces between desorption of $O_2$ into the gas phase and transformation into surface lattice oxygens. The difference in $O_2$ desorption behavior between bulk oxide surfaces and the magnetite surfaces of the present study can be attributed to the magnetite overlayers of this study being supported on a metallic iron substrate. For magnetite overlayers on iron, there is a source of cations at the metal–metal oxide interface which allows cations to diffuse through the oxide overlayer to the oxide surface, as discussed elsewhere (*1*). For bulk oxide surfaces, there is no equivalent source of cations. This enhanced cation availability for the magnetite overlayers on iron favors incorporation of adsorbed oxygen as part of the lattice (by interaction of the diffusion-supplied cations with the lattice additions) over desorption of $O_2$ into the gas phase. This is especially true for the more-strongly-bound atomic species which are stable on the surface at temperatures where cation diffusion rates become significant. The existence of these atomic species was confirmed from $CO_2$ adsorption–desorption studies, as discussed in a later section.

### *Interaction of NO with Magnetite Surfaces*

Temperature-programmed desorption following nitric oxide exposure to magnetite surfaces indicated that, besides desorbing intact, NO underwent surface reaction to form both $N_2O$ and $N_2$. Nitrogen dioxide ($NO_2$) was never detected. In these experiments, $^{15}NO$ was utilized instead of

$^{14}NO$ because the $^{15}N_2O$ and $^{15}N_2$ product molecules have different masses than those of $CO_2$ and CO, two potentially interfering background gases.

Figures 2 and 3 illustrate the desorption spectra and calculated apparent initial coverages, respectively, of NO, $N_2O$, and $N_2$ after 50 L saturation NO exposure at 150 K for surfaces vacuum-annealed at temperatures from 150 to 800 K. The monolayer site concentration was assumed to be $1.1 \times 10^{19}$ sites $m^{-2}$, which is the octahedral cation site (B-site) density of the $Fe_3O_4(100)$ surface. The B-site density is the maximum surface cation density for the (100) surface, which is attained when the topmost layer becomes FeO-like. For the various magnetite surfaces, a broad NO($\alpha$) desorption peak at ca. 365 K is found. This peak temperature remained essentially invariant with respect to changes in surface coverage, and the peak shape and broadness indicate the presence of a distribution of binding states with spectral contributions from ca. 250 to 550 K. In fact, for the 150 K surface, two distinct NO spectral contributions are evident at ca. 300 and 390 K inside the spectral peak envelope. The previously reported behavior of NO on iron oxides and other metal oxide surfaces (*15–20*) suggests that this NO($\alpha$) desorption peak represents nitrosyl species adsorbed on exposed cation sites. The more-strongly-bound species

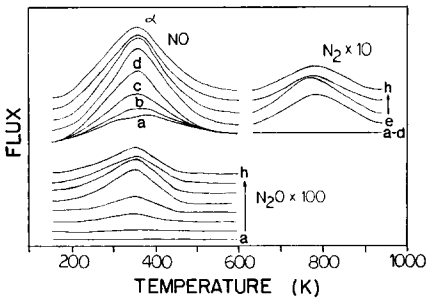


FIG. 2. TPD spectra (65 K $s^{-1}$) of NO, $N_2O$, and $N_2$ desorption from various magnetite surfaces following 50 L saturation NO exposure at 150 K: Surfaces vacuum-annealed at (a) 150 K, (b) 200 K, (c) 300 K, (d) 400 K, (e) 500 K, (f) 600 K, (g) 700 K, and (h) 800 K.

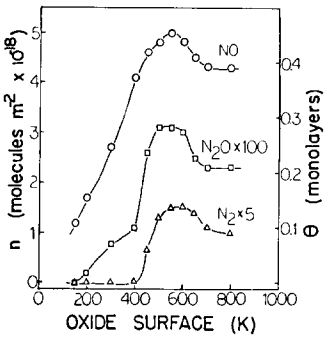


FIG. 3. Apparent initial coverages of desorbed NO, $N_2O$, and $N_2$ species following 50 L saturation NO exposure at 150 K versus the vacuum-annealing temperature of the surface.

are probably associated with cations of lower coordination.

Assuming first-order desorption with a preexponential factor of $10^{13}$ $s^{-1}$ yields an average desorption activation energy $E_d$ of 86 kJ $mol^{-1}$ (for a peak temperature of 365 K) with desorption activation energies ranging from 60 to 130 kJ $mol^{-1}$. The initial $\alpha$-state sticking coefficient $s_0$ at 150 K for all the surfaces was determined to be ca. 0.2, suggestive of nonactivated adsorption ($E_d \cong Q_{NO}$).

The $N_2O$ desorption spectra following NO exposure at 150 K also indicate a broad desorption peak centered at ca. 365 K, which remained invariant with respect to changes in apparent surface coverage. In fact, the $N_2O$ and NO desorption peaks coincide, suggesting that $N_2O$ forms in the same step as NO desorption by a surface-reaction-limited process. It is postulated that this occurs on cation sites of low coordination which can accommodate two adsorbed NO molecules (e.g., formation of dinitrosyl complexes, as reported for the interaction of NO with $Fe^{2+}$ cations supported on silica (*21*) or in zeolites (*22*)). For these types of adsorbed complexes, a competition is imagined between simple desorption of NO molecules and reactive desorption as an $N_2O$ molecule and an adsorbed atomic oxygen species. As displayed in Fig. 3, the amount of NO transformed to $N_2O$ is only ca. 1% of the amount desorbed intact,

suggesting low surface coverages of dinitrosyl-like species and/or low reaction rates compared to desorption rates.

The $N_2$ desorption spectra following exposure of the more-reduced magnetite surfaces to NO at 150 K indicate a broad desorption peak centered at ca. 800 K. This peak temperature decreased with increasing apparent surface coverage. Simultaneous growth of the NO($\alpha$) and $N_2$ desorption peaks upon increasing the NO exposure at 150 K suggested that NO does not dissociate at 150 K to form adsorbed nitrogen and oxygen atoms. Rather, it appears that the amount of desorbed $N_2$ depends on the amount of adsorbed NO, indicating that NO($\alpha$) species are precursors for desorbed $N_2$. During heating, these species either desorb as NO or transform into a more-strongly-bound, dissociated NO state which reacts at higher temperatures to form desorbed $N_2$ and surface lattice oxygen. This state of NO is referred to as $\beta$-state NO. The existence of both weakly-bound and strongly-bound NO species on the iron oxide surface has, indeed, been established by others (*17, 20*).

The shifting of the $N_2$ desorption peak to lower temperatures with increasing NO($\beta$) coverage is suggestive of a desorption process higher than first order. The desorption activation energy for $N_2$ desorption from the NO($\beta$) species was estimated to be ca. 200 kJ $mol^{-1}$ assuming a second-order desorption process with a preexponential factor of $10^{-6}$ $m^2$ $molecules^{-1}$ $s^{-1}$.

The above results suggest that NO is a useful probe molecule for characterizing magnetite surfaces. In particular, Figs. 2 and 3 indicate that the desorption products following saturation NO exposure at 150 K are sensitive to the surface oxidation state. For the NO($\alpha$) state, the saturation coverage increases smoothly ($1.2–4.8 \times 10^{18}$ molecules $m^{-2}$, corresponding to 0.11–0.44 monolayers) as the vacuum-annealing temperature is raised from 150 to 550 K. The NO adsorption capacity thus appears to be related to the number of exposed cation sites. For the desorbed $N_2O$ species, the apparent saturation surface coverage increases in two regimes (see Fig. 3). Upon increasing the vacuum-annealing temperature from 150 to 400 K, the apparent coverage increases smoothly ($0–1.1 \times 10^{16}$ molecules $m^{-2}$, corresponding to 0–0.0010 monolayers). This indicates that the number of cation sites of sufficiently low coordination (to bind two NO molecules) increases with increasing extent of surface reduction. In the second regime, going from the 400 to the 550 K surface, there is a sharper increase in apparent $N_2O$ coverage ($1.1–3.1 \times 10^{16}$ molecules $m^{-2}$, corresponding to 0.0010–0.0028 monolayers). It has been determined by other investigators (*9–13, 23*) that, within this temperature region, the desorption (or incorporation as part of the oxide lattice) of adsorbed atomic oxygen species occurs. Thus, it is postulated that the sharp increase in the number of cation sites of low coordination caused by increasing the vacuum-annealing temperature from 400 to 550 K is related to a decrease in the number of adsorbed atomic oxygen species on these surfaces. This follows from the rationale that the removal of adsorbed $O^-$ species lowers the coordination of the underlying cation sites.

The above behavior is seen more dramatically for the formation of $N_2$. No $N_2$ is produced on the 150–400 K surfaces, which are the more-oxidized surfaces. For the 400 to the 600 K surfaces, $N_2$ is produced in increasing amounts, with NO($\beta$) surface coverages of $0–6.2 \times 10^{17}$ molecules $m^{-2}$, corresponding to 0–0.056 monolayers. This is additional evidence for decreasing surface concentrations of adsorbed $O^{-1}$ species in this temperature region, causing the appearance of lower-coordination cation sites capable of dissociating NO.

Although the increases in the number of desorbed product molecules for the 150 to the 550 K surfaces are readily explained, decreases are observed in the number of desorbed product molecules for higher-temperature surfaces. The fact that de-

creases occur for all product molecules strongly suggests that, above 500–600 K, the model oxide undergoes a surface reconstruction. Thus, new surface planes are postulated to form with lower monolayer adsorption site concentrations. This can be explained by the rationale that the most stable exposed plane for these iron oxide surfaces depends on the amount and nature of the adsorbed oxygen species on these surfaces. For the highly reduced FeO-like surfaces, the preferred exposed plane is probably the (100) plane since it results in a zero net surface ionic charge. In contrast, for the more-oxidized surfaces possessing adsorbed oxygen species, other planes containing higher concentrations of surface cations may be more stable.

It was found that the saturation coverage of NO($\beta$) could be increased by increasing the NO dosing temperature. Figure 4 shows the calculated NO($\alpha$) and NO($\beta$) surface coverages, respectively, for a 600 K surface following 50-L NO exposure at various temperatures. As the dosing temperature is increased from 150 to 250 K, the NO($\beta$) coverage decreases. This decrease indicates that, within this temperature region, no NO($\beta$) species are formed at the time of dosing, and the number of NO($\beta$) species formed is dependent on the surface coverage of NO($\alpha$) species (which decreases with increasing dosing temperature at constant exposure). Thus, it appears that a surface

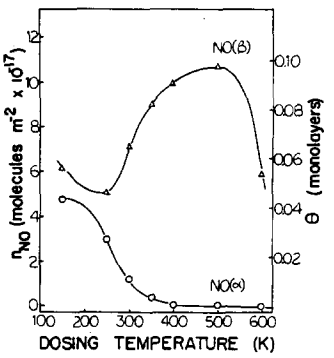


FIG. 4. NO($\alpha$) and NO($\beta$) coverages on a surface vacuum-annealed at 600 K versus dosing temperature for 50 L NO exposure.

temperature of 250 K is not sufficiently high to convert NO($\alpha$) to NO($\beta$). In contrast, increasing the dosing temperature from 250 to 500 K causes an increase in NO($\beta$) surface coverage. In this region, the temperature is apparently high enough to create NO($\beta$) species concomitant with dosing. Adsorbing molecules first form the precursor NO($\alpha$) species which either desorb as NO or are transformed into NO($\beta$). As the dosing temperature is increased, the ratio of the transformation rate to the desorption rate increases. This is evidence that the activation energy for transformation is greater than that for desorption. An approximate value for this difference is estimated to be about 2 kJ mol$^{-1}$ by plotting the 400 and 500 K data points in an Arrhenius fashion. The activation energy for transformation between the $\alpha$-state and $\beta$-state is estimated to be ca. 70 kJ mol$^{-1}$, equal to the desorption activation energy of an NO($\alpha$) species having a peak temperature of 300 K.

Increasing the dosing temperature above 500 K causes a decrease in NO($\beta$) surface coverage. This decrease may be due, in part, to the surface reconstruction postulated earlier, which results in a decrease in monolayer site concentration for surfaces vacuum-annealed higher than ca. 550 K. Moreover, the added complication of $N_2$ desorption from the surface concomitant with high-temperature NO exposures becomes more significant as the dosing temperature is increased above 600 K.

Utilizing a dosing temperature of 400 K and varying the NO exposure of a 600 K surface permitted determination of an initial sticking coefficient for NO($\beta$) formation of $7.8 \times 10^{-5}$. This value is similar to the initial sticking coefficients found for dissociative $N_2$ adsorption on Fe surfaces (*24, 25*). For this system, the low $s_0$ values were attributed both to a low trapping probability (ca. $10^{-2}$) for adsorbing $N_2$ in the molecular precursor state and a much larger preexponential factor for precursor state desorption than for precursor state transformation to the dissociated state. Accordingly, it is

suggested that the low $s_0$ value for NO($\beta$) formation may be due to an approximately four-orders-of-magnitude difference in pre-exponential factors for desorption and transformation pathways. This may also explain the slow rate of NO adsorption often observed on high surface area iron oxides (e.g. (*19, 21*).

### *Interaction of $CO_2$ and CO with Magnetite Surfaces*

The adsorption of $CO_2$ on the various magnetite surfaces yielded no other desorption products than the parent $CO_2$ molecules. Figures 5 and 6 illustrate the $CO_2$ desorption spectra and calculated initial coverages, respectively, for 150–900 K surfaces after 80 L saturation $CO_2$ exposure at 150 K. The monolayer site concentration was taken to be $1.1 \times 10^{19}$ sites $m^{-2}$ (which is both the lattice oxygen density and the B-site cation density of the $Fe_3O_4$(100) surface). No additional, more-strongly-bound $CO_2$ adsorption states were evident for $CO_2$ exposures at high temperatures. The initial $CO_2$ sticking coefficient for all the magnetite surfaces was estimated to be ca. 0.1, suggestive of nonactivated adsorption. The broad $CO_2$ desorption peak (ranging from ca. 200 to 500 K) for all the surfaces suggests that there is a distribution of binding energies. In light of the known adsorption behavior of $CO_2$ on high-surface-area metal oxides (*26–29*), it is proposed that the

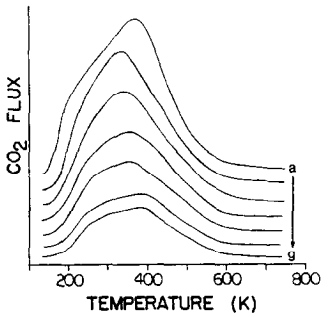


FIG. 5. TPD spectra (50 K $s^{-1}$) of $CO_2$ desorption from various magnetite surfaces after 80 L saturation exposure at 150 K: Surfaces vacuum-annealed at (a) 150 K, (b) 400 K, (c) 500 K, (d) 600 K, (e) 700 K, (f) 800 K, and (g) 900 K.

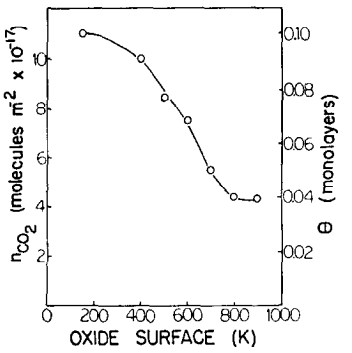


FIG. 6. $CO_2$ coverage following 80 L saturation exposure at 150 K versus the vacuum-annealing temperature of the surface.

$CO_2$ peak represents adsorbed carbonate species. Assuming first-order desorption with a preexponential factor of $10^{13}$ $s^{-1}$ yields desorption energies $E_d$ ($\cong Q_{CO_2}$) ranging from ca. 50 to 120 kJ $mol^{-1}$.

Figures 5 and 6 indicate that both the saturation $CO_2$ coverage and the shape of the $CO_2$ desorption peak depend on the oxidation state of the surface. In particular, the saturation $CO_2$ coverage decreases (from 1.1 to $0.44 \times 10^{18}$ molecules $m^{-2}$, corresponding to 0.10–0.04 monolayers) upon going from the 150 to the 900 K surface. The marked decrease in $CO_2$ coverage upon increasing the vacuum-annealing temperature from 400 to 600 K parallels the postulated decrease in surface coverage of adsorbed atomic oxygen species in this temperature region (*9–13*), suggesting that some of the adsorbed $CO_2$ is associated with atomic oxygen species. The nonzero $CO_2$ coverage for the highly reduced surfaces (annealed at 900 K) also suggests that some $CO_2$ (ca. $4.4–7.5 \times 10^{17}$ molecules $m^{-2}$, corresponding to 0.04–0.07 monolayers) is associated with surface lattice oxygen. These oxygens are probably lattice anions of low coordination on the surface. It should be remembered that part of the decrease in $CO_2$ coverage for the 600 K and higher-temperature surfaces may be due to a decrease in monolayer site concentration from oxide surface reconstruction (as discussed with respect to NO adsorption).

The differences in desorption peak shapes for the various magnetite surfaces indicate differences in the distribution of $CO_2$ adsorption sites. For example, the surface vacuum-annealed at 150 K shows increased relative spectral contributions at ca. 200 and 400 K compared to the desorption spectrum of the 400 K surface (see Fig. 5). It may be anticipated that monodentate carbonate species would have lower binding energies than bidentate (or organic) species since they are only bound to the surface by one as opposed to two oxygens. Thus, it is tempting to assign the spectral contribution at ca. 200 K to monodentate species and that at ca. 400 K to bidentate species. These assignments were investigated using $C^{18}O_2$ to study the exchange of oxygen with the oxide surface. As a monodentate carbonate species, $CO_2$ adsorbs on a surface oxygen site with neither of its oxygen atoms interacting with the oxide surface; therefore, no oxygen exchange should occur between $CO_2$ and the oxide surface. In contrast for bidentate (or organic) carbonate formation, $CO_2$ adsorbs with one of its oxygen atoms participating in the $CO_2$-surface bond. The result is a carbonate species with two oxygens equally bonded to the oxide surface, one oxygen from the original $CO_2$ molecule and one oxygen from the oxide surface. This provides a path for oxygen exchange between $CO_2$ and the oxide surface.

The $C^{18}O^{16}O$, $C^{18}O_2$, and total $CO_2$ desorption spectra from the surface vacuum-annealed at 150 K followed by 80 L $C^{18}O_2$ exposure at 150 K are shown in Fig. 7. These spectra indicate that no oxygen exchange occurs for $CO_2$ desorbing at the lowest temperatures (200–250 K). For $CO_2$ desorbing at higher temperatures, random oxygen exchange occurs as evidenced by approximately equal amounts of desorbed $C^{18}O^{16}O$ and $C^{18}O_2$. These spectra display the desorption behavior that was typical of all the magnetite surfaces, namely, that only the $CO_2$ desorbing on the low-temperature side did so without oxygen exchange.

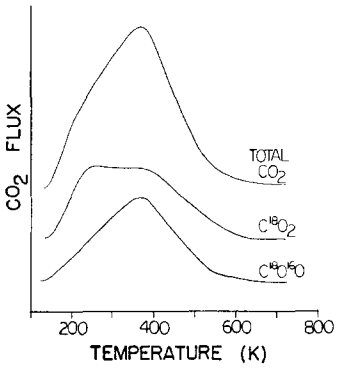


FIG. 7. TPD spectra (50 K $s^{-1}$) of $C^{18}O^{16}O$, $C^{18}O_2$, and total $CO_2$ desorption from the surface vacuum-annealed at 150 K followed by 80 L $C^{18}O_2$ exposure at 150 K.

Thus, it appears that the more-weakly-bound species ($Q_{CO_2}$ = 50–60 kJ $mol^{-1}$) are monodentate carbonate species, and the more-strongly-bound species ($Q_{CO_2}$ = 60–120 kJ $mol^{-1}$) are bidentate carbonate species. From the extent of oxygen exchange on these surfaces, it can be concluded that the majority (ca. 80–90%) of the carbonate species formed are bidentate species. It is important to note that no double oxygen exchange occurred over any of the magnetite surfaces (i.e., no $C^{16}O_2$ was formed), indicating that the bidentate carbonate species were bound to particular adsorption sites below their desorption temperature without $CO_2$ or atomic oxygen migration across the surface.

The participation of adsorbed surface oxygen in carbonate formation was further investigated using $^{18}O_2$. In particular, a 600 K surface (synthesized with $^{16}O_2$) was exposed to 200 L $^{18}O_2$ at 150 K followed by 80 L $C^{16}O_2$. The resulting $C^{18}O^{16}O$, $C^{16}O_2$, and total $CO_2$ desorption spectra are shown in Fig. 8. The total $CO_2$ desorption spectrum is similar in peak shape and saturation surface coverage (ca. $1.0 \times 10^{18}$ molecules $m^{-2}$, corresponding to 0.091 monolayers) to the desorption spectrum from a 150 K surface exposed to 80 L $CO_2$ at 150 K. The coverage by bidentate carbonate species containing $^{18}O$ was estimated to be ca. $3.0 \times 10^{17}$ molecules $m^{-2}$, calculated

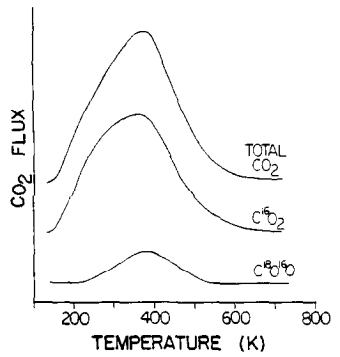


FIG. 8. TPD spectra (50 K $s^{-1}$) of $C^{18}O^{16}O$, $C^{16}O_2$, and total $CO_2$ desorption from the surface vacuum-annealed at 600 K followed by sequential exposure to 200 L $^{18}O_2$ then 80 L $C^{16}O_2$ at 150 K.

by multiplying by two the coverage calculated from the $C^{18}O^{16}O$ desorption spectrum. The total bidentate carbonate coverage was estimated to be ca. $8 \times 10^{17}$ molecules $m^{-2}$ by fitting the desorption spectrum with peaks at 200 and 400 K, and assuming that the latter peak was due to bidentate species. These coverages indicate that approximately 40% of the bidentate carbonate species formed involved participation from surface atomic oxygen deposited from $^{18}O_2$. In a similar experiment, a 400 K surface (synthesized with $^{16}O_2$) was subjected to the same exposures of $^{18}O_2$ and $C^{16}O_2$ at 150 K. The total $CO_2$ desorption spectrum was similar to the spectrum of Fig. 8, but no appreciable desorption of $C^{18}O^{16}O$ occurred. Thus, it appears that no atomic $^{18}O$ species were deposited on the 400 K surface, the surface already being saturated with atomic $^{16}O$ species during synthesis. The results of these experiments are further indications that for magnetite surfaces vacuum-annealed at 400–600 K, adsorbed atomic oxygen species exist and participate in bidentate carbonate formation.

It may be suggested that bidentate carbonate formation requires the presence of a cation–anion pair site. It appears, however, that the number of reactive surface oxygen species governs the number of bidentate carbonate species. This follows from the observation (see Fig. 6) that the $CO_2$ coverage decreases as the vacuum-annealing temperature increases. Yet, the role of cation sites adjacent to surface oxygen species in the formation of carbonate species was demonstrated by $CO_2$ and NO coadsorption experiments. Desorption spectra for $CO_2$ and NO were collected for two different surfaces: a surface vacuum-annealed at 400 K and sequentially exposed to 50 L NO and 80 L $CO_2$ at 150 K, and a 400 K surface sequentially exposed to 80 L $CO_2$ and 50 L NO at 150 K. For the NO-predosed surface, $CO_2$ adsorption was totally inhibited except for a low coverage (ca. $4 \times 10^{16}$ molecules $m^{-2}$, corresponding to 0.004 monolayers) of monodentate carbonate species. The corresponding NO desorption spectrum was identical to that from a 400 K surface exposed to 50 L NO. The inhibition of $CO_2$ adsorption suggested that NO($\alpha$) species are adsorbed on surface cation sites normally utilized for bidentate carbonate formation. Moreover, the suppression of the number of monodentate carbonate species formed suggested that the presence of adsorbed NO($\alpha$) species on the oxide surface may affect the surrounding surface oxygen sites. For the $CO_2$-predosed surface, NO adsorption was partially inhibited as evidenced by a 20% decrease (equivalent to ca. $8 \times 10^{17}$ molecules $m^{-2}$) in the NO desorption peak intensity. The corresponding $CO_2$ desorption spectrum was identical to that from a 400 K surface exposed only to 80 L $CO_2$. In addition, the bidentate carbonate coverage on this surface was approximately equal to the decrease in NO saturation coverage. This is further evidence that the surface cation sites participating in bidentate carbonate formation are also sites normally utilized for NO adsorption.

Monodentate carbonate formation was found on all surfaces but was enhanced for the most-oxidized (150 K) surface. This can be explained by the fact that the 150 K surface possesses the most-basic surface sites, since it has been reported (*29*) that strong

basicity is required for monodentate carbonate formation.

In contrast to $CO_2$ adsorption, exposure of the magnetite surfaces to CO resulted in only weak adsorption. Figure 9 shows both the CO desorption spectra and the calculated initial coverages for surfaces vacuum-annealed at 150–600 K followed by 50 L saturation CO exposure at 150 K. A single CO desorption peak is observed, having a peak temperature of ca. 200 K which remains invariant with respect to changes in surface coverage. This peak is assigned to a weakly-bound carbonyl species in accordance with the known adsorption behavior of CO on metal oxide surfaces (*29–33*). Assuming nonactivated adsorption and first-order desorption with a preexponential factor of $10^{13}$ $s^{-1}$ yields a heat of adsorption $Q_{CO} \cong 46$ kJ $mol^{-1}$. This is similar to $Q_{CO} \cong 50$ kJ $mol^{-1}$ found for CO adsorbed in a carbonyl fashion on ZnO surfaces (*33*). Yet, the desorption spectra are in disagreement with those of Kelemen *et al.* (*23*) who indicated stronger CO adsorption (with a desorption peak as high as 415 K) and higher CO coverages (0.10–0.20 monolayers) for FeO-like surfaces vacuum-annealed at 650 K. Matching their experimental conditions for the magnetite surfaces in the present study resulted in negligible CO adsorption. At this time, there is no explanation for this discrepancy.

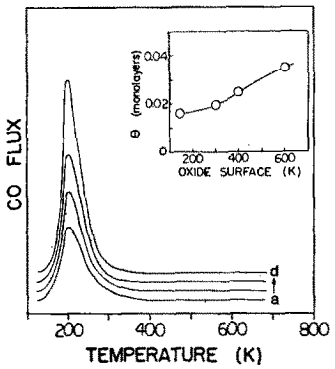


FIG. 9. TPD spectra (50 K $s^{-1}$) of CO desorption from various magnetite surfaces after 50 L saturation exposure at 150 K: Surfaces vacuum-annealed at (a) 150 K, (b) 300 K, (c) 400 K, and (d) 600 K. Corresponding surface coverages are plotted in the inset.

The saturation CO coverages found for the magnetite surfaces vacuum-annealed at 150–600 K are small (ca. $1.6–3.9 \times 10^{17}$ molecules $m^{-2}$, corresponding to 0.015–0.035 monolayers). The coverage increases as the vacuum-annealing temperature is increased (i.e., the surface becomes more reduced), suggesting that there is a correlation between CO coverage and the number of exposed cation sites. Moreover, the CO coverages are similar to NO($\beta$) coverages obtained after saturation NO exposure at 150 K. This suggests that the sites for CO adsorption are similar to those for NO($\beta$) formation, these being surface cations of low coordination. It is possible that weaker CO adsorption can occur on the more-highly-coordinated cation sites, but this could not be observed in this study due to the minimum-surface-temperature limit of the TPD apparatus.

## CONCLUSIONS

The adsorptive properties of magnetite surfaces of differing oxidation state (produced by vacuum-annealing at temperatures from 150 to 950 K) were studied with respect to various probe molecules ($O_2$, NO, $CO_2$, CO) using temperature-programmed desorption. The different oxide surfaces were found to possess different amounts and types of adsorbed oxygen species. Surfaces vacuum-annealed at temperatures higher than 600 K possessed only strongly bound, lattice-like oxygen species. In addition to these species, the 600 to 300 K surfaces possessed increasing surface coverages of less-strongly-bound atomic oxygen species, in agreement with the increasing oxidation state determined by XPS (*1*). Finally, surfaces vacuum-annealed at temperatures below 300 K also possessed weakly bound molecular oxygen species ($Q_{O_2} \cong 61$ and 78 kJ $mol^{-1}$).

Nitric oxide possessed two adsorption states designated as $\alpha$ and $\beta$ states. The NO($\alpha$) species (nitrosyl species with $Q_{NO} \cong$

60–130 kJ $mol^{-1}$) desorbed intact. A small number (ca. 1%) of these species desorbed reactively as $N_2O$, leaving surface oxygen. This suggested the presence of dinitrosyl adsorption complexes. The NO($\beta$) species (more-strongly-bound, dissociated species) reacted to form $N_2$ ($E_d \cong 200$ kJ $mol^{-1}$) and surface lattice oxygen. Both NO($\alpha$) and NO($\beta$) coverages increased with increased extent of surface reduction suggesting that adsorbed NO was associated with surface cation sites. The formation of $N_2$ and $N_2O$ was believed to originate from NO adsorbed on cation sites of low coordination. Total NO coverages indicated that NO adsorption may be useful for titrating exposed cation sites.

Carbon dioxide adsorbed on the oxide surfaces as carbonate species ($Q_{CO_2} \cong 50$–120 kJ $mol^{-1}$). For the more-strongly-bound species ($Q_{CO_2} \cong 60$–120 kJ $mol^{-1}$), desorption of both $C^{18}O^{16}O$ and $C^{18}O_2$ occurred following $C^{18}O_2$ adsorption. This suggested that these species were adsorbed as bidentate (or organic) carbonates capable of exchanging oxygen with the surface. Surface oxygen species participating in this exchange were probably adsorbed atomic oxygen species and lattice-like oxygen species of low coordination. For the more-weakly-bound species ($Q_{CO_2} \cong 50$–60 kJ $mol^{-1}$) no oxygen exchange occurred, suggesting that these species were adsorbed as monodentate carbonates. The majority (ca. 80–90%) of the carbonate species on the oxide surfaces were bidentate carbonate species. The total $CO_2$ coverage decreased with increased extent of surface reduction. Bidentate carbonate formation was believed to require the presence of a cation–anion pair site, although the number of reactive surface oxygen species appeared to govern the number of bidentate species formed. The importance of cation sites adjacent to the surface oxygen species for the formation of bidentate carbonate species was demonstrated by the observation that preadsorption of NO on cation sites blocked $CO_2$ adsorption. In addition, preadsorption of $CO_2$ on these sites inhibited NO adsorption. Monodentate carbonate formation was enhanced for the more-oxidized surfaces indicating that strongly basic adsorption sites were required.

Carbon monoxide adsorbed only weakly on the oxide surfaces ($Q_{CO} \cong 46$ kJ $mol^{-1}$). The increasing CO coverage with increasing extent of surface reduction suggested that CO adsorbed in a carbonyl fashion on surface cation sites of low coordination.

ACKNOWLEDGMENTS

We are grateful to the National Science Foundation for financial support of this work and for providing a Graduate Fellowship to one of us (TJU). We thank Gregory Raupp for valuable assistance during the latter stages of this work.

REFERENCES

1. Udovic, T. J., and Dumesic, J. A., *J. Catal.* **89,** 303 (1984).
2. Udovic, T. J., Ph.D. thesis, University of Wisconsin-Madison, 1982.
3. Benziger, J., and Madix, R. J., *Surf. Sci.* **94,** 119 (1980).
4. UTI 100C Operating Manual, Uthe Technology International, Sunnyvale, Calif., 1975.
5. Bozso, F., Ertl, G., Grunze, M., and Weiss, M., *Appl. Surf. Sci.* **1,** 103 (1977).
6. Wedler, G., Geuss, K. P., Colb, K. G., and McElhiney, G., *Appl. Surf. Sci.* **1,** 471 (1978).
7. Wedler, G., Colb, K. G., McElhiney, G., and Heinrich, W., *Appl. Surf. Sci.* **2,** 30, (1978).
8. Yoshida, K., and Somorjai, G. A., *Surf. Sci.* **75,** 46 (1978).
9. Halpern, B., and Germain, J. E., *J. Catal.* **37,** 44 (1975).
10. Gillot, B., and Ferriot, J. F., *Chem. Scr.* **11,** 121 (1977).
11. González-Cruz, L., Joly, J., and Germain, J., *J. Chim. Phys.* **75,** 324 (1978).
12. Iwamoto, M., Yoda, Y., Yamazoe, N., and Seiyama, T., *J. Phys. Chem.* **82,** 2564 (1978).
13. Yang, B. L., and Kung, H. H., *J. Catal.* **75,** 329 (1982).
14. Bielański, A., and Haber, J., *Catal. Rev.* **19,** 1 (1979).
15. Otto, K., and Shelef, M., *J. Catal.* **18,** 184 (1970).
16. Contour, J. P., and Mouvier, G., *J. Catal.* **40,** 342 (1975).
17. Sazonova, S., Alikina, G. M., Glazneva, G. V., Keier, N. P., Bogdanchikova, N. E., and Devytov, V. G., *Kinet. Katal.* **18,** 441 (1977).

*18.* Glazneva, G. V., Davydov, A. A., Sazonova, I. S., Shchekochikhin, Y. M., and Keier, N. P., *React. Kinet. Catal. Lett.* **9,** 131 (1978).
*19.* Lund, C. R. F., Schorfheide, J. J., and Dumesic, J. A., *J. Catal.* **57,** 105 (1979).
*20.* Busca, G., and Lorenzelli, V., *J. Catal.* **72,** 303 (1981).
*21.* Yuen, S., Chen, Y., Kubsh, J. E., Dumesic, J. A., Topsøe, N., and Topsøe, H., *J. Phys. Chem.* **86,** 3022 (1982).
*22.* Segawa, K. I., Chen, Y., Kubsh, J. E., Delgass, W. N., Dumesic, J. A., and Hall, W. K., *J. Catal.* **76,** 112 (1982).
*23.* Kelemen, S. R., Kaldor, A., and Dwyer, D. J., *Surf. Sci.* **121,** 45 (1982).
*24.* Boszo, F., Ertl, G., and Weiss, M., *J. Catal.* **49,** 18 (1977).
*25.* Ertl, G., Lee, S. B., and Weiss, M., *Surf. Sci.* **114,** 515 (1982).
*26.* Amerikov, V. G., and Kasatkina, L. A., *Kinet. Katal.* **12,** 165 (1971).
*27.* Knözinger, H., "Advances in Catalysis," Vol. 25, p. 184. Academic Press, New York, 1976.
*28.* Pajares, J. A., González de Prado, J. E., García Fierro, J. L., González Tejuca, L., and Weller, S. W., *J. Catal.* **44,** 421 (1976).
*29.* Morterra, C., Ghiotti, G., Boccuzzi, F., and Coluccia, S., *J. Catal.* **51,** 299 (1978).
*30.* Zecchina, A., Coluccia, S., Guglielminetti, E., and Ghiotti, G., *J. Phys. Chem.* **75,** 2774 (1971).
*31.* Rubene, N. A., Davydov, A. A., Kravtsov, A. V., Usheva, N. V., and Smol'yaninov, S. I., *Kinet. Katal.* **17,** 400 (1976).
*32.* Kozub, G. M., Voroshilov, I. G., Roev, L. M., and Rusov, M. T., *Kinet. Katal.* **17,** 1040 (1976).
*33.* Gay, R. R., Nodine, M. H., Henrich, V. E., Zeiger, H. J., and Solomon, E. I., *J. Amer. Chem. Soc.* **102,** 6752 (1980).